Available online at www.sciencedirect.com
ScienceDirect
ELSEVIER
JOURNAL OF RARE EARTHS, Vol. 35, No. 2, Feb. 2017, P. 193
JOURNAL OF RARE EARTHS
www.re-journal.com/en/

Effect of combinative addition of mischmetal and titanium on the microstructure and mechanical properties of hypoeutectic Al-Si alloys used for brazing and/or welding consumables

WANG Bo (王 博)[1], XUE Songbai (薛松柏)[1,*], WANG Jianxin (王俭辛)[2], LIN Zhongqiang (林中强)[3]

(1. College of Materials Science and Technology, Nanjing University of Aeronautics and Astronautics, Nanjing 210016, China; 2. Jiangsu Provincial Key Laboratory of Advanced Welding Technology, Jiangsu University of Science and Technology, Zhenjiang 212003, China; 3. Zhejiang Yuguang Aluminum Material Co., Ltd., Jinhua 321200, China)

Received 18 May 2016; revised 29 June 2016

Abstract: Effects of mischmetal (RE) and/or Ti modifier on the microstructure including α-Al dendrites, eutectic Si phases and other secondary phases of Al-Si brazing and/or welding alloys were investigated by differential scanning calorimetry (DSC), optical microscopy (OM), scanning electron microscopy (SEM). The DSC results showed that an addition of RE decreased the eutectic temperature and caused supercooling, promoting the nucleation of eutectic Si crystals. In addition, the maximum temperature of the first endothermic peak varied with the different RE contents, which had a good correlation with the microstructural modification of the eutectic Si phase. The α-Al dendrites were well refined by increasing the cooling rate or adding 0.08 wt.% of Ti. When 0.05 wt.% RE was added to the Al-5Si-0.08Ti alloy, the morphology of eutectic Si phase was transformed from coarse platelet to fine fibers and the mechanical properties of the resulting welding rod were well improved. Whereas, when excess RE was added, a large number of β-Fe phases appeared and the aspect ratios of β-Fe phases increased. The morphologies and chemical components of two kinds of RE-containing intermetallic compounds (IMCs) were also discussed.

Keywords: Al-Si alloy; rare earths; modification; microstructure; mechanical properties

With industrial technology advancing nowadays, welding consumables with excellent qualities are desperately required all over the world. Al-Si series brazing and/or welding alloys, designed for joining heat-treatable aluminum alloys, are playing a decisive role in both the military and commercial fields.

Al-Si brazing and/or welding alloys have lower melting point and more fluidity (wetting action) than 5XXX series welding alloys, which result in low sensitivity to weld cracking with 6XXX series base alloys and produce bright, almost smut free welds. Among Al-Si brazing and/or welding alloys, hypoeutectic (as ER4043) and near eutectic compositions (as ER4047) have attracted strong attentions of the welders and researchers[1]. Elrefaey et al.[2] studied the different effects of ER4043 and ER5356 on the microstructures of dissimilar 6082/5182 joints using cold metal transfer (CMT) welding. It was found that comparing the weld metal (WM) grain sizes of the two welding alloys, the grains were smaller when ER4043 was used, and the average WM grain size in the cases of dissimilar joints welded with ER4043 and ER5356 were 164 and 217 μm, respectively. Dewan et al.[3] studied the influences of postweld heat treatment (PWHT) on tensile properties of gas tungsten arc (GTA) welded aluminum alloy AA6061-T651 joints, and showed that ER4043 welding rod was very suitable for GTA welding of aluminum alloy AA6061. It was also found that the WM responded to postweld solution treatment followed by aging, namely the mechanical properties of ER4043 welds could be improved by appropriate PWHT.

Due to the above characteristics, Al-Si series welding wires and rods were recommended by American Bureau of Shipping (ABS) and other authorities for welding the wrought aluminum alloys like AA3003, AA5052, AA6061 and the casting aluminum alloys like A214, A356, etc.[4]. However, pronounced deficiencies still can be seen in the domestic ones, including high drawing broken-line rate, poor wire feeding, high porosity and poor mechanical properties of welded joints[5], which urgently need to be solved.

Iron is one of the most important impurities in aluminum and Fe can improve high temperature short-time strength, creep strength and hardness at high and room temperature of aluminum alloy. It was reported that Al-Si eutectic alloy for pressure casting often required a

Foundation item: Project supported by National Natural Science Foundation of China (51375233), Priority Academic Program Development (PAPD) of Jiangsu Higher Education Institutions, China Postdoctoral Science Foundation (2014M550289, 2015T80548)

* **Corresponding author:** XUE Songbai (**E-mail:** xuesb@nuaa.edu.cn; **Tel.:** +86-25-84896070)

DOI: 10.1016/S1002-0721(17)60899-8

certain amount of Fe added to facilitate casting off from the mold, thereby improving the surface quality of the casting[6]. However, during the manufacturing process of Al-Si welding wire and rod, the content of Fe was strictly controlled for the majority of the Fe being present in the form of intermetallic compounds (IMCs), and the coarse flake-like β-Fe IMCs would separate the aluminum substrate and deteriorate significantly the room-temperature performance of the Al-Si alloy[7–10].

Titanium is a good grain refiner. The α-Al grains of as-cast Al-Si alloy can be refined by adding the element Ti[11]. However, it was demonstrated that Ti had little effect on the eutectic Si phase in Al-Si alloy. The current researches focus on adding element Sr into the casting Al-Si alloy, which facilitates the transformation of eutectic Si phase from original lamellar or long needle-like into fine fibrous, thereby improving the mechanical properties of the Al-Si alloy[12]. However, the addition of Sr increased the hydrogen absorption tendency of aluminum melt[13], resulting in the increasing of hydrogen content of aluminum welding wire or rod itself. It was easy to obtain poor quality welded joints with high porosity using this kind of Al-Si welding wire or rod.

Rare earth elements, known as the "vitamins" of metal materials, in recent years, show significant modification effects on Al-Si alloys. Studies pointed out that rare earth can also refine the aluminum melt and depress the hydrogen absorption, improving the quality of aluminum melt[14–16]. However, current researches focus on the modification effect of rare earth element on the structural parts such A356 alloy, microstructure and mechanical properties of Al-Si welding wire or rod with rare earth modified were rarely reported. In this study, the novel Al-Si based welding alloys with combinative addition of mischmetal (RE) and Ti were prepared and the effects of Ti and RE on the microstructure and mechanical properties of Al-Si welding rods were investigated.

1 Experimental

Al-5Si (AS) alloy for experimental was prepared using commercially pure aluminum (99.7% Al), Al-20Si master alloy, Al-10RE alloy and titanium metal additive (75% Ti). Alloy melting and melt purification were carried out in a graphite crucible muffle furnace at 700–760 ºC. Melt was refined using hexachloroethane (C_2Cl_6) and degassed with pure argon. The nominal and actual chemical compositions of welding alloys with varied contents of Ti and/or RE are listed in Table 1.

The melt was poured into a pre-baked pig mold and solidified into a circular cross ingot after a certain time of heat preservation. To study the effect of cooling rate, two different preheat temperatures and cooling conditions of the mold were used. In the first case, the mold was preheated to 500 ºC, and after pouring, the mold was cooled in atmospheric air. This arrangement provided a low cooling rate with a secondary dendrite arm spacing (SDAS) of 38–46 μm. In the second case, the mold was preheated to 150 ºC. The melt was poured into the mold, and the latter was cooled by water to provide a higher solidification rate or low SDAS value (22–28 μm). These cooling rates, corresponding to SDAS values of 22–28 and 38–46 μm, are referred to as "high" and "low" cooling rates relative to each other. Aluminum welding rods with a diameter of 9.5 mm were subsequently prepared by hot-extrusion of the cylindrical ingots.

Table 1 Nominal and actual chemical compositions of the studied welding alloys (wt.%)

Sample No.	Si	Fe	Ti		RE		Al
			Nominal	Actual	Nominal	Actual	
AS	5.0	0.18	0	0	0	0	Bal.
AST	5.0	0.18	0.08	0.081	0	0	Bal.
AST-1	5.0	0.18	0.08	0.085	0.01	0.012	Bal.
AST-2	5.0	0.18	0.08	0.083	0.05	0.049	Bal.
AST-3	5.0	0.18	0.08	0.079	0.10	0.104	Bal.
AST-4	5.0	0.18	0.08	0.078	0.20	0.211	Bal.

Thermal analysis was performed using the Netzsch® STA 449 F3 and the DSC and TG data were obtained simultaneously at a 10 ºC/min heating rate under the atmosphere of nitrogen. The cylindrical ingots and hot-extruded welding rods with different components were prepared into metallographic samples, and microstructures were observed using the TV-400D type metallographic microscope and ZEISS ΣIGMA field emission scanning electron microscope coupled to an energy dispersion X-ray (FE-SEM/EDX). Tensile specimens with a gauge length of 100 mm were prepared from 9.5 mm hot-extruded welding rods and the tensile tests were performed with a 3 mm/min loading rate at room temperature using an electronic WDW-20 universal testing machine.

2 Results and discussion

2.1 Thermal analysis

From the DSC curve of the heating process (Fig. 1(a)), two endothermic peaks appeared below the liquidus. According to the Al-Si binary phase diagram, two reactions occurred in turn with the temperature increasing: peak 1 corresponded to the melting of eutectic Si phase, peak 2 corresponded to the melting of α-Al dendrites. The AST-*x*RE alloys (x=0, 0.01, 0.05, 0.1, 0.2, 0.65) had only two endothermic peaks, and no explicit peak related to the precipitation of RE-containing phases could be detected using the DSC technique, the same results were demonstrated by Alkahtani et al.[17] using thermal analysis of solidification process.

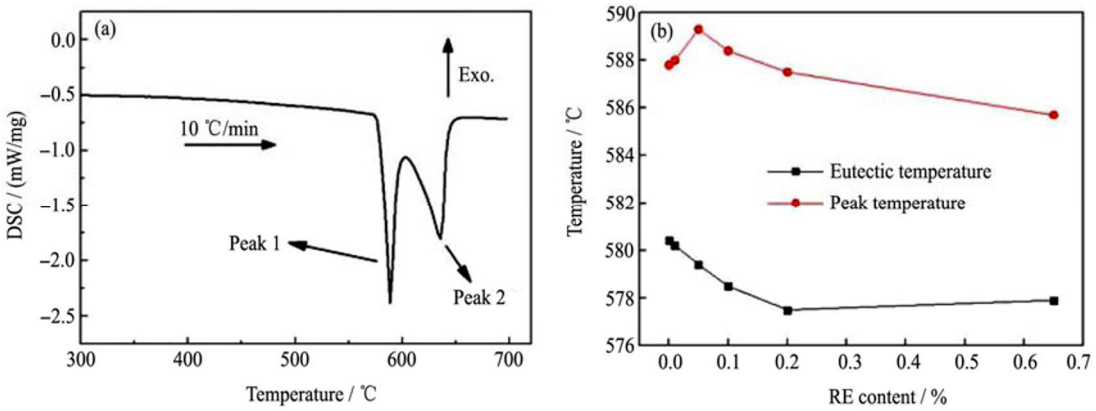

Fig. 1 (a) Typical DSC curve of AST-2 at a heating rate of 10 ºC/min; (b) Characteristic temperatures of AST-*x*RE alloys (*x*=0, 0.01, 0.05, 0.1, 0.2, 0.65): eutectic temperature and summit temperature of peak 1

The characteristic data of DSC curve changed with at the different heating rates, so the heating rate was set at 10 ºC/min. It can be seen from Fig. 1(b), that the eutectic temperature of eutectic Si phase decreases with the increasment of RE contents, when the RE content exceeds 0.2 wt.%, the eutectic temperature remains unchanged. Kang et al. revealed that the decline of the eutectic temperature caused the crystallization of the eutectic Si to take place at a high undercooling degree, then affected the nucleation rate and growth kinetics of the eutectic Si crystal and resulted in a good modified effect[18]. Thus, addition of RE into Al-Si welding alloy can modify the eutectic Si phase by decreasing the eutectic temperature and inducing undercooling.

In addition, the summit temperature of peak 1, namely the peak temperature, which was calculated by the Netzsch® Proteus software, had a close relation with eutectic modification. When the content of RE was 0.05 wt.%, the peak temperature reached the maximum value. When the content of RE was higher than 0.05 wt.%, with the increasing of RE content, the peak temperature continued to decrease. The peak temperature evolution was in good agreement with the microstructure evolution of Al-Si ingots and welding rods with varied RE contents discussed in section 2.3. Peak temperature showed the point with the highest heat absorption rate, the value of which can be used to represent the eutectic growth and part of nucleation. When the eutectic Si phases were small in their size and distributed uniformly, it required enough heat to implement the melting of a large number of small eutectic Si phases, which can be used for explaining the correlation between the evolution of the peak temperature and modification efficiency of RE on eutectic Si phase. Farahany et al.[19] also found a good correlation between the results of thermal and microstructural analysis. Based on the above analysis, the thermal analysis method can be used for the rough determination of the modification efficiency of RE on the Al-Si welding alloy.

2.2 Effects of different cooling rates and Ti additions on the microstructures of as-cast AS alloys

The microstructures of as-cast AS alloys with different cooling rates and contents of Ti are shown in Fig. 2. In the absence of Ti and under a slow cooling condition, coarse columnar α-Al dendrites were found as shown in Fig. 2(a). When adding 0.08 wt.% Ti into the as-cast AS alloy solidified under a slow cooling condition, the α-Al dendrites were refined (Fig. 2(b)). The microstructure of as-cast AS alloy solidified without Ti addition and under a fast cooling condition is shown in Fig. 2(c), compared with Fig. 2(a, b), the mean size of α-Al dendrites was the smallest, indicating that the cooling rate was an important factor affecting the size of α-Al dendrites. Fig. 2(d) shows that the microstructure of as-cast AST alloy solidified under a fast cooling condition and the α-Al dendrites were further refined compared with the microstructure of Fig. 2(c).

The effect of Ti on α-Al dendrites was mainly because of $TiAl_3$ particles, which were produced from the peritectic reaction of the aluminum melt and Ti. $TiAl_3$ particles, which were effective heterogeneous substrates for formation of α-Al dendrites, can increase the nucleation rate of α-Al dendrites and hence lead to the refinement of α-Al dendrites. The size of α-Al dendrites can be represented by the SDAS. Increasing the cooling rate decreased the SDAS because of the following reasons: (1) Increasing the cooling rate increased the constitutional under cooling. This condition caused the formation of more secondary dendrite arms. (2) Increasing the cooling rate caused the interface of the liquid and solid to move faster. Consequently, ratios of area to volume of dendrite arms should increase in order to facilitate the heat extraction. (3) Increasing the cooling rate decreased the thickness of dendrite, because there was not enough time for ripening and coalescence of dendrite.

Fig. 3 shows the high magnification microstructures of as-cast AST alloys with different cooling rates. From Fig. 3(a, b), it can be seen that the needle-like mor-

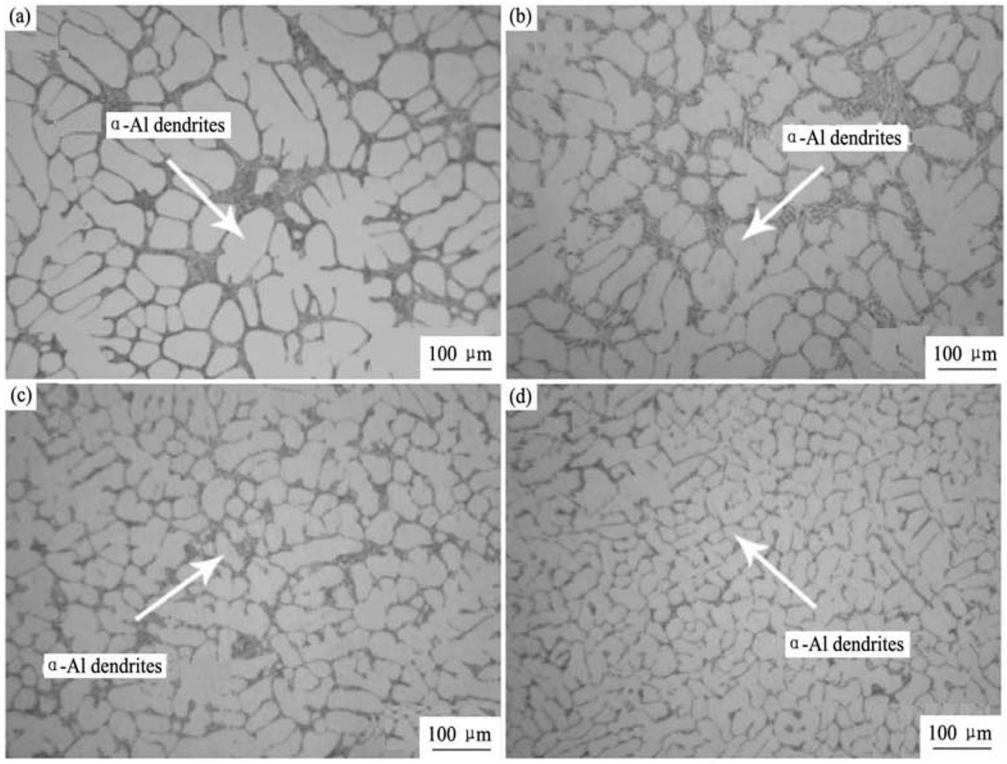

Fig. 2 Microstructures of as-cast AS alloys with different cooling rates and different contents of Ti: (a) low rate, 0 Ti; (b) low rate, 0.08 Ti; (c) high rate, 0 Ti; (d) high rate, 0.08 Ti

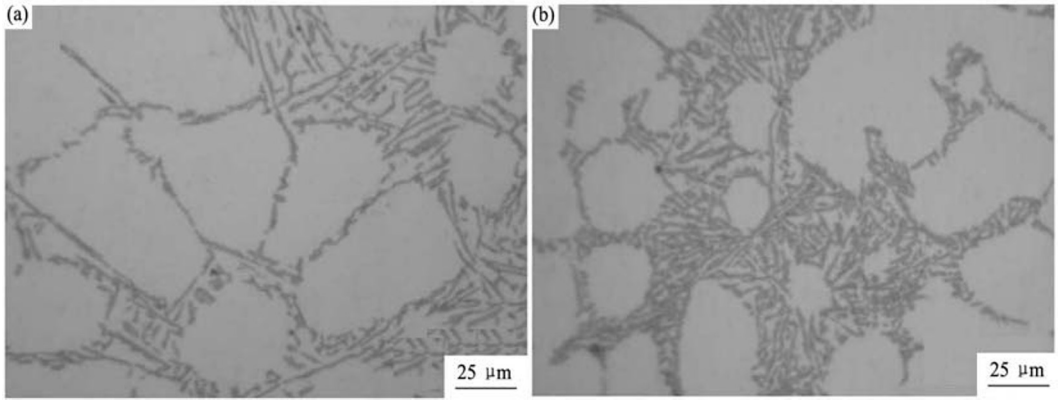

Fig. 3 High magnification microstructures of as-cast AST alloys with different cooling rates: (a) low rate; (b) high rate

phology of eutectic Si phase predominate in the as-cast AST alloy, which suggested that Ti addition had no effect on the morphology of eutectic Si phase or the effect was not obvious. While increasing the cooling rate, the aspect ratio of eutectic Si phase was decreased. It indicated that rapid cooling can not only significantly refine the α-Al dendrites, but also modify the morphology of eutectic Si phase to a limited extent. The reasons for the modification of cooling rate on morphology of eutectic Si phase are as follows: (1) The increase in the proportion of large and elongated particles with a slow solidification was simply due to the increased diffusion distance. The eutectic Si particles thus became coarser and longer. (2) Increasing cooling rate during solidification decreased the SDAS and subsequently divided the eutectic liquid into many small pockets rather than the large eutectic regions presented in the low cooling rate structure. As a result, the aspect ratio of eutectic Si particle in the more rapidly solidified alloys was decreased.

2.3 Effect of combinative addition of RE and Ti on the morphology of eutectic Si phase

Fig. 4 shows the varied SEM microstructures of as-cast AST-xRE alloys. As can be seen from Fig. 4(a–c), the aspect ratio of eutectic Si phase decreased with the increasing of the RE addition (0 wt.%–0.05 wt.%), and the morphology of eutectic Si phase shifted from large platelet to short rod-like or fine fiber. The morphology evolution of eutectic Si phase can be explained through Fig. 5. As shown in Fig. 5, with increasing the RE content, the coarse needle-like eutectic Si phases progressively branched and broke up, lamellar Si phases with small size were first formed, then the size became smaller and the number increased. The separating phe-

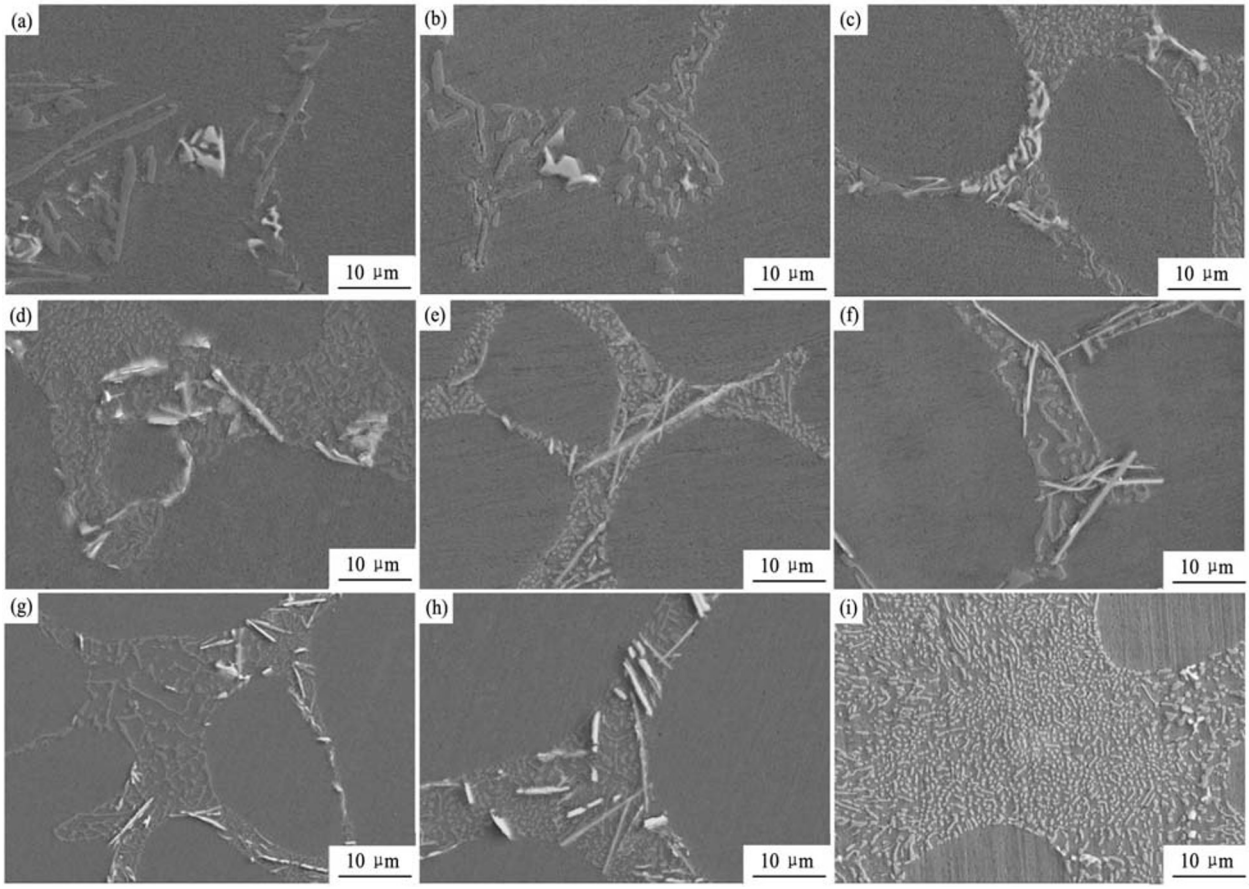

Fig. 4 SEM microstructures of as-cast AST-*x*RE alloys: (a) *x*=0; (b) *x*=0.01; (c) *x*=0.05; (d) *x*=0.1; (e) *x*=0.2 fully-modified zone; (f) *x*=0.2 partially-modified zone; (g) *x*=0.65 at low magnification; (h) *x*=0.65 at high magnification; (i) microstructure of AST-0.02Sr for comparison

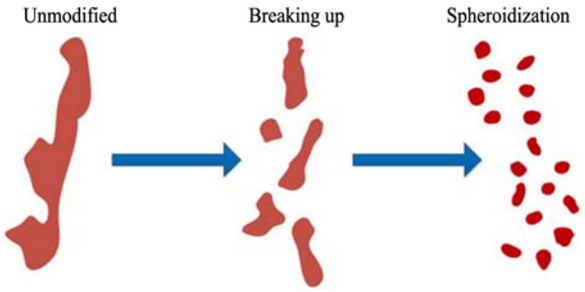

Fig. 5 Schematic characterization of RE modification on the eutectic Si phase in the RE-containing AST alloy

nomenon stopped in the final stage. The Si phases were subjected to spheroidization. The boundaries of the Si phases became smooth.

Under conventional casting conditions, the eutectic Si phase, with the characteristic of small flat growth, grew rapidly along the <112> direction into lamellar or coarse acicular eutectic Si crystals[8]. Once the orientation growth was inhibited by additions of the chemical modifier, the Si phases would turn to grow in the form of small granules. It was reported that additions of the chemical modifiers easily produced twin defects in the Si crystals, the repeated twining made the growth reorientate, thus, the fibers Si phases can bend, curve and split to create finer particles[20]. One theory for the effect was that atoms of the modifier absorbed onto the growth steps of the silicon solid-liquid interface and it was supported by the observation that modifiers became concentrated in the silicon, not in the aluminum phase. Lu and Hellawell[20] declared that when the atomic radius ratio of the modifier element and silicon was close to 1.65, a growth twin would be caused by the element at the interface. Mischmetal was mainly composed of cerium (Ce) and lanthanum (La), both of which met the restriction of atomic radius ratio. So it was easy for mischmetal to enrich in front of the eutectic Si cells and modify the morphology of eutectic Si phase. Another reason for explaining the mechanism of modification was that RE elements of La and Ce additions also yielded the undercooling degree[21] degree and so delayed the nucleation of eutectic Si phases, leading to the refinement of the eutectic Si phases[22].

When the RE content increased to 0.1 wt.% (Fig. 4(d)), the size of eutectic Si phase remained unchanged, however, RE enriched at the grain boundaries and the short rod-like RE-rich IMCs were precipitated close to eutectic Si phases. The fact that the size of eutectic Si phase stayed unchanged may be because that the modification capacity of RE element itself reached the saturation state, and another possible reason was that excess RE element of free state segregated and reacted with Al, Si elements

and formed the coarse RE-rich IMCs, which had no effect on the modification of the eutectic Si phase.

Further increasing the RE content to 0.2 wt.%, the effect of element RE on the eutectic Si phase exhibited two different conditions: fully modified and partially modified. When the white RE-rich IMCs were small, namely the segregation of RE element was not serious, and the eutectic Si phase was small and was evenly distributed (Fig. 4(e)) in the fully-modified condition. While in the area where large needle-like white RE-rich IMCs were precipitated, the eutectic Si phase was partially modified, and the size of eutectic Si phase was large and the distribution was uneven (Fig. 4(f)). When an excess RE content (0.65 wt.%) was added into the AST alloy, the size and number of RE-rich IMCs became larger, which seriously deteriorated the modification effect on eutectic Si phases, and some areas lack of RE exhibited platelet morphology of eutectic Si phase (Fig. 4(g, h)). Fig. 4(i) shows the modification effect of 0.02 wt.% Sr on the eutectic Si phase in the AST alloy. Compared with the SEM microstructure of AST alloy modified by Sr, the modification efficacy of RE element on eutectic Si phase was relatively low. Tsai et al.[23] also reported the huge gap between Sr modification and rare earth element La modification, indicating that the modification efficiency in microstructures and mechanical properties of A356 alloy with 1.0 wt.% La were similar to those modified by the commercial modifier, 0.012 wt.% Sr.

Fig. 6 shows the microstructures of hot-extruded AST-*x*RE welding rods (*x*=0, 0.01, 0.05). As can be seen from Fig. 6(a, b), the grains were refined evidently by hot extrusion and the eutectic Si phase could not be distinguished clearly in metallographic scale. Moreover, obvious orientation was observed in the longitudinal- sectional microstructure of hot-extruded welding rods. When no RE was added (Fig. 6(c)), the mean size of eutectic Si particles was 3.35 μm. While 0.01 wt.% RE was added into the welding rod, the mean size of eutectic Si particles was reduced to 2.14 μm (Fig. 6(d)). When the RE content further increased to 0.05 wt.% (Fig. 6(e)), the mean size of eutectic Si particles was 0.96 μm, and the morphology of eutectic Si phase shifted from coarse rod-like form to the fine dot-like form. Under the same conditions, the SEM microstructure of hot-extruded AST-0.02Sr welding rod is shown in Fig. 6(f), and the mean size of eutectic Si particles was 0.50 μm, which was only half of that of AST-0.05RE welding rods.

The microstructure evolution of AST-*x*RE welding rods was similar to that of as-cast AST-*x*RE alloys, which gave further support to the modification benefit of RE addition to eutectic Si phases and can be used for explaining the changes in mechanical properties of AST-*x*RE welding rods discussed in section 2.5.

2.4 Effects of combinative additions of RE and Ti on the morphology of Fe-rich IMCs

The solid-state solubility of Fe in Al was very low, so the majority of Fe existed in the form of IMCs in aluminum alloy and the nature which depended mainly on the alloy elements present[24]. According to the chemical compositions and the temperature of the Fe-rich IMCs, Fe may be precipitated as IMC with varied morphologies, the most common being polyhedral crystals, "Chinese scripts" and thin platelets.

Under rapid cooling conditions, the morphologies of RE-rich IMCs and Fe-rich IMCs which are shown in Fig. 7

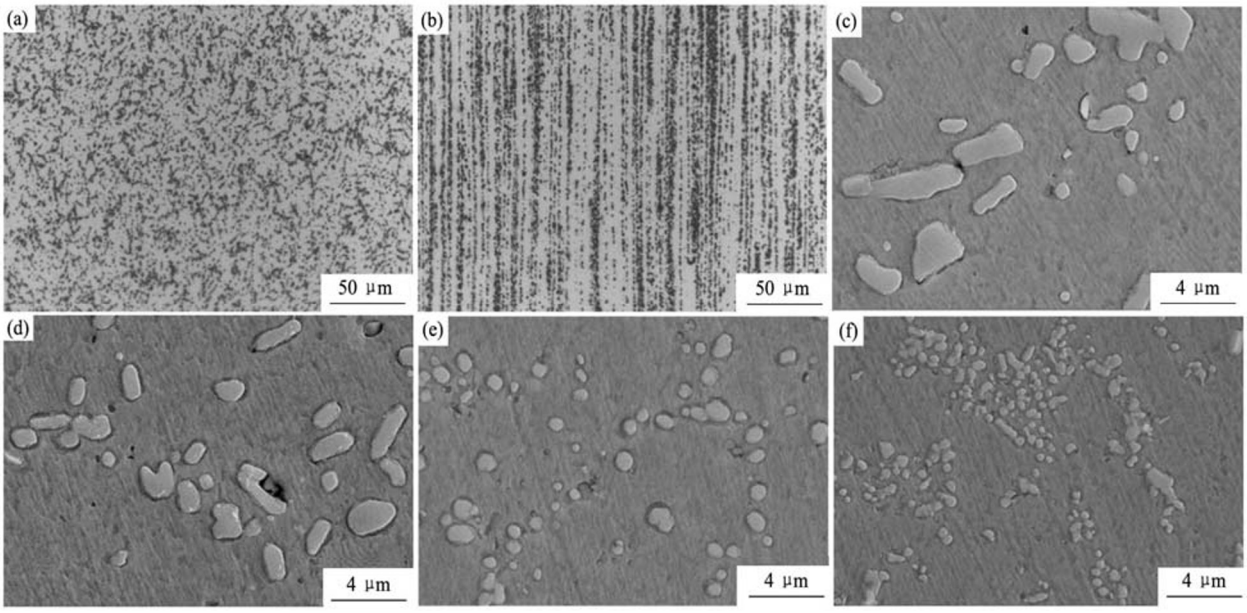

Fig. 6 Microstructures of hot-extruded AST-*x*RE welding rods

(a) *x*=0.05, cross-sectional metallographic structure; (b) *x*=0.05, longitudinal-sectional metallographic structure; (c) *x*=0, cross-sectional SEM structure; (d) *x*=0.01, cross-sectional SEM structure; (e) *x*=0.05, cross-sectional SEM structure; (f) SEM microstructure of hot-extruded AST-0.02Sr welding rod for comparison

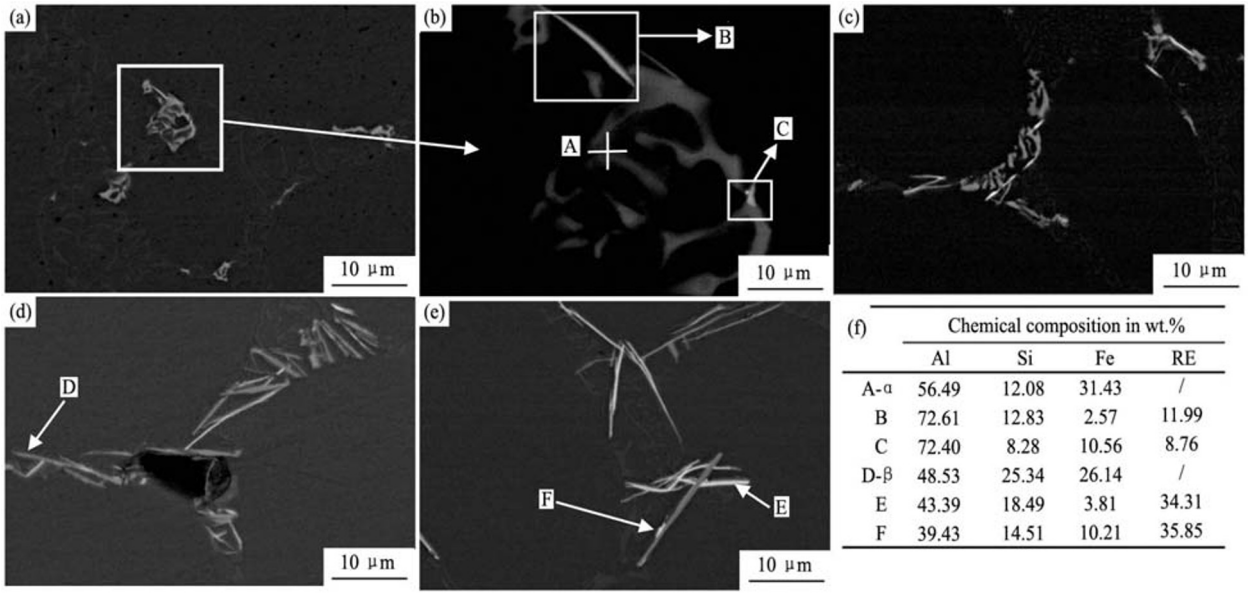

(f)

	Chemical composition in wt.%			
	Al	Si	Fe	RE
A-α	56.49	12.08	31.43	/
B	72.61	12.83	2.57	11.99
C	72.40	8.28	10.56	8.76
D-β	48.53	25.34	26.14	/
E	43.39	18.49	3.81	34.31
F	39.43	14.51	10.21	35.85

Fig. 7 RE-rich IMCs and Fe-rich IMCs of as-cast AST-*x*RE alloys

(a) *x*=0.01; (b) *x*=0.01 at high magnification; (c) *x*=0.05; (d) *x*=0.1; (e) *x*=0.2; (f) EDS data of point A-F in Fig. 7

changed with increasing RE contents. As can be seen from Fig. 4(a), (b) and Fig. 7(a), when no RE element was added or RE content was low (not more than 0.05 wt.%), light gray Fe-rich IMCs mainly existed in the form of Chinese-script which were identified as α-Fe phases by the composition analysis (Point A in Fig. 7(b)). In addition, from Fig. 7(b), another short rod-like white phase was found and determined as RE-rich IMC by the EDS data of Point B and C in Fig. 7. In consideration of the fact that the position where one kind of IMC precipitated was close to that of another, it can be concluded that a certain kind of the phase (Fe-rich IMC or RE-rich IMC) provided the nucleation substrate for another phase (RE-rich IMC or Fe-rich IMC).

When the RE content further increased to 0.1 wt.%–0.2 wt.%, the RE-rich IMCs showed long needle-like structures, and the morphology of Fe-rich IMCs transformed from Chinese script-like α-Fe phases to platelet β-Fe phases, which could be confirmed from the EDS analysis of Point A and D in Fig. 7. Thus, combined the analysis of section 2.3, it could be found that adding excess RE element led to the serious segregation of RE in the AST alloy, which resulted in the formation of needle-like RE-rich IMCs and deteriorated the modification effects of RE elements on the eutectic Si phase. In addition, the presence of an excess of RE element also caused the transformation from α-Fe phase to β-Fe phase, which may severely decrease the ductility of AST alloy.

In general, the length of needle β-Fe phase can be decreased by reducing the Fe content or increasing the cooling rate[25]. The alloys prepared in this study only contained 0.18 wt.% Fe, which was much smaller than the Fe content of ternary eutectic arrest (0.8 wt.% Fe) in Al-Si-Fe alloy, furthermore, all the AST alloys with the additions of different RE elements were prepared under the high cooling rate condition, so in accordance with the general principles, the length of β-Fe phases should be quite small. However, large number of long needle β-Fe phases were found in the AST alloys with excess RE modification, which indicated that the RE element changed the nucleation or growth step of β-Fe phases to some extent. Besides, as can be seen from Fig. 7(d), the void that appeared in the microstructure of AST-0.1RE was associated with the needle-like β-Fe phase, this correlation was also found and explained by other researchers[26].

Besides, the distinction of the morphology between the α-Fe phase and the β-Fe phase was mainly due to the difference of chemical compositions, which can be found through the EDS data of Fe-rich IMCs. When the mass fraction ratio of Fe to Si (Fe/Si) was greater than 1, Fe-rich IMCs tended to form the Chinese script structure, while the Fe/Si ratio was close to 1, Fe-rich IMCs tended to form the long needle-like structure. A similar law was also found in the relationship between chemical compositions and the morphology of RE-rich IMCs, except that the elements involving in the ratio calculation were different. When the mass fraction ratio of RE to Fe (RE/Fe) was close to 1, the size of irregular RE-rich IMCs was small, which had little impact on the mechanical properties of the AST alloy. With RE/Fe ratio increasing, RE-rich IMCs showed needle-like structures. When the aspect ratio of RE-rich IMCs increased, the size of RE rich IMCs became larger, and the adverse effects of microstructure on the mechanical properties of AST alloy were more and more serious.

2.5 Effects of cooling rates and RE contents on the mechanical properties of AST welding rods

Tensile properties of different hot-extruded welding rods with varied chemical compositions under different

Table 2 Variations in tensile properties of different hot-extruded welding rods at different cooling rates

No.	Cooling rate	Welding rods	Tensile strength/MPa	Elongation/%
1	Low	AS	123	5.2
2	Low	AST	129	7.4
3	High	AST	142	25.1
4	High	AST-1	143	28.2
5	High	AST-2	149	33.3
6	High	AST-3	151	27.4
7	High	AST-4	143	22.0

conditions of cooling rates are shown in Table 2. As shown in Table 2, AS welding rod under low cooling rate conditions presented the lowest tensile strength and elongation. Under the low cooling rate condition, the SDAS of as-cast alloy was large, and the grains of the alloy were still relatively coarse even though the alloy was hot-extruded. The alloys with large and elongated particles showed high strain hardening and, thus, had a high damage accumulation rate by particle cracking. Through the observation of the tensile fracture surface (Fig. 8(a)) in which there was a large volume fraction of coarse grains, and the fracture mechanism was identified as brittle fracture (the elongation was only 5.2%). While in the AST alloy under low cooling rates, α-Al grains were refined by Ti addition and mechanical properties including strength and elongation were improved to some extent, however, the ductility of the alloy was still poor (the elongation was only 7.4%), which could be supported by the comparison of Fig. 2(a, b). Besides, the "river pattern" was observed in the tensile fracture surface of AST welding rods under a low cooling rate (Fig. 8(b)), which indicated that the fracture mechanism was still brittle fracture, belonging to cleavage fracture in a specific classification.

The tensile strength (142MPa) and elongation (25.1%) of the AST welding rods under a high cooling rate, which had small SDAS in cast state and was refined by hot-extrusions, increased by 10% and 239%, respectively, compared with those of AST welding rods prepared at a low cooling rate. For metal materials, the more the number of fine dimples and more uniform the distribution was, the better the ductility of the metal was. As can be seen from Fig. 8(c), there existed a large number of fine dimples in the tensile fracture surface, which indicated that the fracture mechanism was attributed to the ductile fracture.

Under high cooling rate conditions, increasing the amount of RE element (0.01 wt.%–0.20 wt.%), the tensile strength and the elongation of AST-*x*RE welding rods increased first and then decreased. However, the RE content corresponding to the turning point of the tensile strength was different from that of the elongation. The reason for this phenomenon was that when the RE content was 0.1 wt.%, more hard and brittle needle-like IMCs (including Fe-rich IMCs and RE-rich IMCs) were formed in the microstructures, which increased the strength and hardness of the alloy to a certain degree, while at the same time the increased volume fraction and size of the Fe-IMCs and RE-IMCs further separated the matrix and worsened the ductility of the alloy, so the elongation declined. While further increasing the RE content to 0.20 wt.%, platelet and fibrous eutectic Si phases coexisted in

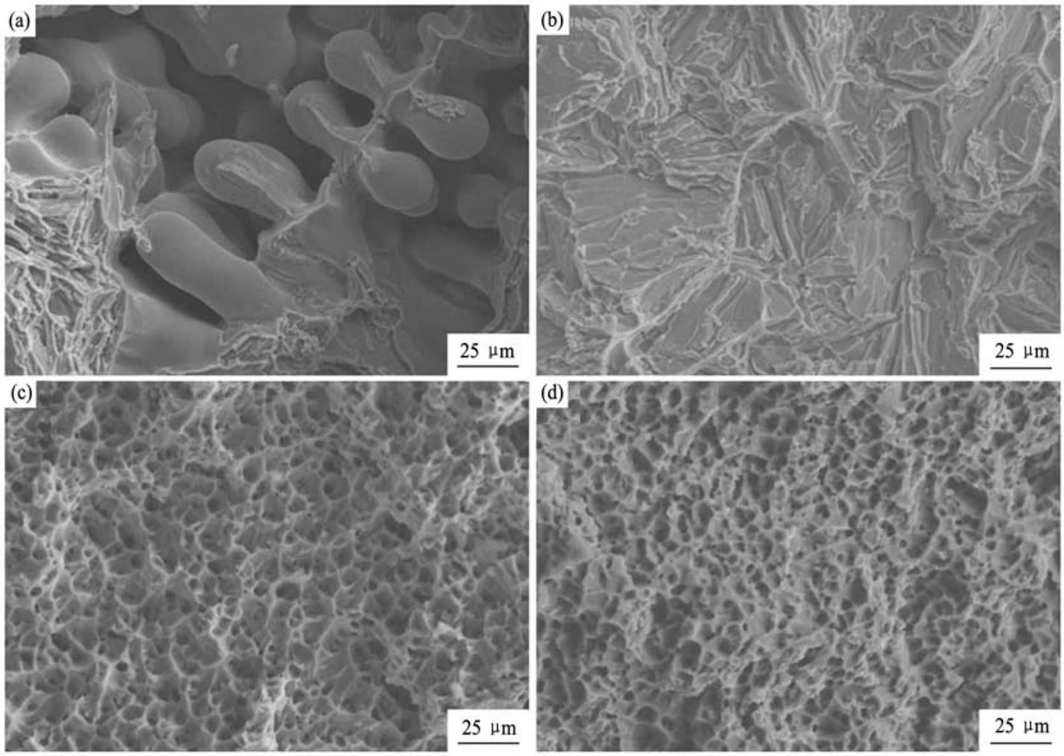

Fig. 8 Tensile fracture surfaces of AS welding rods at a low cooling rate (a), AST welding rods at a low cooling rate (b), AST welding rod at a high cooling rate (c) and AST-2 welding rod at a high cooling rate (d)

the AST-0.2RE alloy, when the aspect ratio of RE-rich IMCs increased, needle-like RE-rich IMCs and Fe-rich IMCs were interdependent or staggered, and the region where platelet eutectic Si phase existed or needle-like IMCs enriched was likely to be the area of stress concentration, in which crack was first initiated and rapidly propagated, resulting in the decrease of the tensile strength of the AST welding rod.

As can be seen from the fracture morphologies in Fig. 8, the biggest influential factor is the cooling rate, followed by chemical compositions of the alloy (namely alloying). When the alloy was produced under a rapid cooling rate, α-Al dendrites were refined and eutectic Si phases were modified to a limited extent, and the fracture mechanism shifted from brittle fracture to ductile fracture, and a large number of dimples appeared in the tough fracture.

3 Conclusions

In this study, the effects of RE and Ti on the microstructures evolution of Al-Si alloys used for brazing and/or welding consumables and mechanical properties of hot-extruded welding rods with the diameter 9.5 mm was investigated. The results showed that:

(1) The eutectic temperature of eutectic Si phase decreased with proper RE addition, causing the crystallization of the eutectic Si phase to take place at a high undercooling degree and then leading to a good modified effect.

(2) Addition of 0.08 wt.% Ti could only refine the α-Al dendrites, which had no effect on the morphology of eutectic Si phases or the effect was not obvious.

(3) A combinative addition of 0.08 wt.% Ti and 0.05 wt.% RE could not only refine the α-Al dendrites, but also fully modify the morphology of the eutectic Si phase.

(4) The morphologies and chemical compositions of other secondary phases such as RE-rich IMCs and Fe-rich IMCs changed with the increasing of the RE addition. The increased volume fraction and size of the eutectic Si phases, Fe-rich IMCs or RE-rich IMCs were responsible for the lower ductility of the Al-Si alloys.

References:

[1] Ramanaiah N, Rao K S, Guha B, Rao K P. Effect of modified AA4043 filler on partially melted zone cracking of Al-alloy gas tungsten arc welds. *Sci. Technol. Weld. Join*., 2005, **10**: 591.

[2] Elrefaey A, Ross N G. Microstructure and mechanical properties of cold metal transfer welding similar and dissimilar aluminum alloys. *Acta Metall. Sin. (Engl. Lett.)*, 2015, **28**(6): 715.

[3] Dewan M W, Wahab M A, Okeil A M. Influence of weld defects and postweld heat treatment of gas tungsten arc-welded AA-6061-T651 aluminum alloy. *J. Manuf. Sci. E.–T. ASME*, 2015, **137**(5): 051027.

[4] Sun H H, Xue S B, Feng X M, Lin Z Q, Li Y. Microstructure and mechanical properties of weld joint of marine 6082 aluminum alloy by TIG welding. *Trans. China Weld. Inst*., 2014, **35**(2): 91.

[5] Ambriz R, Barrera G, García R, López V. The microstructure and mechanical strength of Al-6061-T6 GMA welds obtained with the modified indirect electric arc joint. *Mater. Des*., 2010, **31**(6): 2978.

[6] Suárez-Peña B, Asensio-Lozano J. Influence of Sr modification and Ti grain refinement on the morphology of Fe-rich precipitates in eutectic Al-Si die cast alloys. *Scr. Mater*., 2006, **54**(9): 1543.

[7] Yan H, Chen F H, Li Z H. Microstructure and mechanical properties of AlSi10Cu3 alloy with (La+Yb) addition processed by heat treatment. *J. Rare Earths*, 2016, **34**(9): 938.

[8] Ma Z, Samuel A, Doty H, Valtierra S, Samuel F. Effect of Fe content on the fracture behavior of Al-Si-Cu cast alloys. *Mater. Des.*, 2014, **57**: 366.

[9] Samuel E, Samuel A, Doty H, Valtierra S, Samuel F. Intermetallic phases in Al-Si based cast alloys: new perspective. *Int. J. Cast Met. Res*., 2014, **27**(2): 107.

[10] Li Z H, Yan H. Modification of primary α-Al, eutectic silicon and β-Al_5FeSi phases in as-cast AlSi10Cu3 alloys with (La+Yb) addition. *J. Rare Earths*, 2015, **33**(9): 995.

[11] Haro-Rodríguez S, Goytia-Reyes R E, Dwivedi D K, Baltazar-Hernández V H, Flores-Zúñiga H, Pérez-López M J. On influence of Ti and Sr on microstructure, mechanical properties and quality index of cast eutectic Al-Si-Mg alloy. *Mater. Des*., 2011, **32**(4): 1865.

[12] Timpel M, Wanderka N, Kumar G V, Banhart J. Microstructural investigation of Sr-modified Al–15 wt.% Si alloys in the range from micrometer to atomic scale. *Ultramicroscopy*, 2011, **111**(6): 695.

[13] Liu L, Samuel A M, Samuel F H, Doty H W, Valtierra S. Influence of oxides on porosity formation in Sr-treated Al-Si casting alloys. *J. Mater. Sci*., 2003, **38**(6): 1255.

[14] Xing P F, Gao B, Zhuang Y X, Liu K H, Tu G F. Effect of erbium on properties and microstructure of Al-Si eutectic alloy. *J. Rare Earths*, 2010, **28**(6): 927.

[15] Aguirre-De la Torre E, Pérez-Bustamante R, Camarillo-Cisneros J, Gómez-Esparza C, Medrano-Prieto H, Martínez-Sánchez R. Mechanical properties of the A356 aluminum alloy modified with La/Ce. *J. Rare Earths*, 2013, **31**(8): 811.

[16] Ouyang Z Y, Mao X M, Hong M. The influence of strontium and rare earth elements on the surface oxide film's protective effect of A356 aluminum alloy melt. *Foundry*, 2006, **10**: 18.

[17] Alkahtani S A, Elgallad E M, Tash M M, Samuel A M, Samuel F H. Effect of rare earth metals on the microstructure of Al-Si based alloys. *Materials*, 2016, **9**(1): 45.

[18] Kang H S, Yoon W Y, Kim K H, Kim M H, Yoon Y P, Cho I S. Effective parameter for the selection of modifying agent for Al-Si alloy. *Mater. Sci. Eng., A*, 2007, **449**: 334.

[19] Farahany S, Ourdjini A, Idris M H. The usage of com-

puter-aided cooling curve thermal analysis to optimise eutectic refiner and modifier in Al-Si alloys. *J. Therm. Anal. Calorim.*, 2011, **109**(1): 105.

[20] Lu S Z, Hellawell A. The mechanism of silicon modification in aluminum-silicon alloys: Impurity induced twinning. *Metal. Trans. A*, 1987, **18**(10): 1721.

[21] Tsai Y C, Lee S L, Lin C K. Effect of trace Ce addition on the microstructures and mechanical properties of A356 (Al-7Si-0.35Mg) aluminum alloys. *J. Chin. Inst. Eng.*, 2011, **34**(5): 609.

[22] Shankar S, Riddle Y W, Makhlouf M M. Eutectic solidification of aluminum-silicon alloys. *Metall. Mater. Trans. A*, 2004, **35**(9): 3038.

[23] Tsai Y C, Chou C Y, Lee S L, Lin C K, Lin J C, Lim S W. Effect of trace La addition on the microstructures and mechanical properties of A356 (Al-7Si-0.35 Mg) aluminum alloys. *J. Alloys Compd*., 2009, **487**(1): 157.

[24] Rana R S, Purohit R, Das S. Reviews on the influences of alloying elements on the microstructure and mechanical properties of aluminum alloys and aluminum alloy composites. *Int. J. Sci. Res. Publ*., 2012, **2**(6): 1.

[25] Narayanan L A, Samuel F H, Gruzleski J E. Crystallization behavior of iron-containing intermetallic compounds in 319 aluminum alloy. *Metall. Mater. Trans. A*, 1994, **25**(8): 1761.

[26] Moustafa M A. Effect of iron content on the formation of β-Al_5FeSi and porosity in Al-Si eutectic alloys. *J. Mater. Process Technol.*, 2009, **209**(1): 605.